Title
Intercepting fleeting cyclic allenes with asymmetric nickel catalysis

Journal
Nature, 586(7828)

ISSN
0028-0836

Authors
Yamano, Michael M
Kelleghan, Andrew V
Shao, Qianzhen
et al.

Publication Date
2020-10-08

DOI
10.1038/s41586-020-2701-2

Peer reviewed

Published in final edited form as:

Nature. 2020 October ; 586(7828): 242–247. doi:10.1038/s41586-020-2701-2.

Intercepting fleeting cyclic allenes with asymmetric nickel catalysis

Michael M. Yamano[#1], **Andrew V. Kelleghan**[#1], **Qianzhen Shao**[#1], **Maude Giroud**[1], **Bryan J. Simmons**[1], **Bo Li**[1], **Shuming Chen**[1], **K. N. Houk**[1,✉], **Neil K. Garg**[1,✉]

[1]Department of Chemistry and Biochemistry, University of California, Los Angeles, Los Angeles, CA, USA

[#] These authors contributed equally to this work.

Abstract

Strained cyclic organic molecules, such as arynes, cyclic alkynes and cyclic allenes, have intrigued chemists for more than a century with their unusual structures and high chemical reactivity[1]. The considerable ring strain (30–50 kilocalories per mole)[2,3] that characterizes these transient intermediates imparts high reactivity in many reactions, including cycloadditions and nucleophilic trappings, often generating structurally complex products[4]. Although strategies to control absolute stereochemistry in these reactions have been reported using stoichiometric chiral reagents[5,6], catalytic asymmetric variants to generate enantioenriched products have remained difficult to achieve. Here we report the interception of racemic cyclic allene intermediates in a catalytic asymmetric reaction and provide evidence for two distinct mechanisms that control absolute stereochemistry in such transformations: kinetic differentiation of allene enantiomers and desymmetrization of intermediate π-allylnickel complexes. Computational studies implicate a catalytic mechanism involving initial kinetic differentiation of the cyclic allene enantiomers through stereoselective olefin insertion, loss of the resultant stereochemical information, and subsequent introduction of absolute stereochemistry through desymmetrization of an intermediate π-allylnickel complex. These results reveal reactivity that is available to cyclic allenes beyond the traditional cycloadditions and nucleophilic trappings previously reported, thus expanding the types of product accessible from this class of intermediates. Additionally, our computational studies suggest two potential strategies for stereocontrol in reactions of cyclic allenes. Combined, these results lay the foundation for the development of catalytic asymmetric reactions involving these classically avoided strained intermediates.

✉**Correspondence and requests for materials** should be addressed to K.N.H. or N.K.G.; houk@chem.ucla.edu; neilgarg@chem.ucla.edu.

Author contributions M.M.Y., A.V.K., M.G. and B.J.S. designed and performed experiments and analysed experimental data. Q.S., B.L. and S.C. designed, performed, and analysed computational data. K.N.H. and N.K.G. directed the investigations and prepared the manuscript with contributions from all authors; all authors contributed to discussions.

Online content

Any methods, additional references, Nature Research reporting summaries, source data, extended data, supplementary information, acknowledgements, peer review information; details of author contributions and competing interests; and statements of data and code availability are available at https://doi.org/10.1038/s41586-020-2701-2.

Competing interests The authors declare no competing interests.

Supplementary information is available for this paper at https://doi.org/10.1038/s41586-020-2701-2.

Arynes, cyclic alkynes and cyclic allenes have captured the attention of the scientific community for more than a century[1]. The field originated with Stoermer and Kahlert's controversial proposal of 2,3-benzofuranyne's (**1**) existence in 1902[7] (Fig. 1a). Fifty years later, Roberts[8] and Wittig[9,10] independently validated the intermediacy of benzyne (**2**), prompting extensive theoretical and experimental studies[1]. The related intermediates cyclohexyne (**3**) and 1,2-cyclohexadiene (**4**) were discovered soon thereafter and were shown to engage in similar strain-promoted reactivity[11,12]. Intermediates **2**–**4** exhibit high strain energies, ranging from 30–50 kcal mol^{-1} (refs. [2,3]) and, consequently, high reactivities and short lifetimes[13,14]. Nowadays, these classes of strained cyclic intermediates, particularly arynes, are used in the synthesis of heterocycles[15], drug scaffolds[16], ligands for catalysis (such as XPhos)[17], natural products[18–20], agrochemicals[21] and organic materials[22].

Despite the many modern synthetic applications of transient strained intermediates, the development of catalytic asymmetric reactions of these species has remained challenging. So far, only two strategies exist, which are the palladium-catalysed [2+2+2] cycloaddition of arynes to form helically chiral products[23,24] and the α-arylation of in-situ-generated chiral enamines with electrochemically generated arynes[25]. Overall, catalytic asymmetric strategies for controlling absolute stereochemistry in the trapping of strained cyclic intermediates are rare, particularly those suitable for the formation of stereodefined sp^3 centres.

Cyclic allenes are attractive building blocks because trapping can occur under mild conditions and lead to the formation of two new bonds, with the creation of one or more sp^3 centres[26–31]. Moreover, the inherent axial chirality of cyclic allene intermediates and the relatively facile interconversion of enantiomers could provide an opportunity to achieve asymmetric reactions through a dynamic kinetic resolution (DKR)[32]. Pioneering studies by Balci and jones showed that cyclic allenes can racemize on a timescale that outcompetes their trapping (Fig. 1b), a requisite feature of the envisioned DKR process[33]. Specifically, upon generating enantioenriched cyclic allene **6** from enantioenriched allene precursor (+)−**5**, only the racemic cycloadduct (±)−**7** is obtained as a result of rapid racemization of allene **6**. This observation, coupled with previous results from our own group[27], prompted our design of the enantioselective process shown in Fig. 1c. Racemic silyl triflate allene precursor **8** can be converted into a racemic mixture of allenes **9** and **ent-9** upon exposure to a fluoride source. We expected these enantiomers to interconvert rapidly before selective interception of one allene enantiomer in a catalytic asymmetric reaction. Overall, such a process would convert racemic silyl triflate **8** into enantioenriched product **11** via a DKR.

To explore the proposed strategy, we sought to identify a suitable catalytic reaction capable of efficiently and selectively intercepting the cyclic allene. As metal-catalysed reactions of strained cyclic allenes are almost unknown[26,34], we identified several criteria for initial reaction discovery. The reaction selected for our study would ideally: (1) be compatible with conditions for strained intermediate generation, (2) allow for the facile in situ generation of an organometallic intermediate in catalytic quantities, and (3) be amenable to the development of an asymmetric variant. With these requirements in mind, the denitrogenative annulation of benzotriazinones[35] was deemed an attractive reaction manifold. Such annulations have been demonstrated to be compatible with fluoride-mediated generation of

transient species, such as arynes[36]. Furthermore, oxidative addition into benzotriazinones **12** is known to proceed rapidly and irreversibly to form metallacycle **14** (Fig. 1d), which we envisioned should provide a sufficient concentration of **14** to intercept short-lived allene **9** (ref. [37]). Lastly, elegant asymmetric variants employing linear allenes have also been reported by Murakami[38].

Having identified the ideal system in which to test our hypothesized DKR, we pursued the specific transformation shown in Fig. 1d, wherein benzotriazinones **12** would react with racemic strained cyclic allene precursors **8** to provide tricyclic products **13**. However, several challenges posed by the transformation shown in Fig. 1d should be noted. First, the fleeting allene intermediate **9** and the catalytically generated metallacycle **14**, two species present in low concentrations, must react with one another. Additionally, to render the transformation enantioselective via the envisioned DKR, racemization of allene **9** must outcompete olefin insertion. Lastly, in the olefin insertion step, organometallic species **14** must preferentially react with a single allene enantiomer to provide enantioenriched metallacycle **15**, en route to product **13**.

Towards the development of this enantioselective reaction, we first sought to establish the feasibility of a racemic variant (Fig. 2). After optimization, we found that a variety of benzotriazinones **16** and allene precursors **17** underwent the desired annulation. Reactions proceeded optimally when using $Ni(cod)_2$ as precatalyst, 1,1′-bis(diphenylphosphino)ferrocene (DPPF) as ligand, and cesium fluoride as the fluoride source in acetonitrile at 35 °C. Reactions occurred smoothly using 1:1 stoichiometry between benzotriazinones **16** and silyl triflates **17**. Notably, we did not observe olefin isomerization of products **19** or **20** to provide the corresponding aromatic products at any point during reaction development. With regard to the scope of the benzotriazinone annulation partner, various nitrogen substituents were tolerated, including *p*-tolyl, *p*-fluorophenyl, methyl and a removable benzyl group, as demonstrated by the formation of annulated products **21**–**24**. Additionally, both electron-rich and electron-deficient benzotriazinones could be used in the transformation, as evidenced by products **25** and **26**. Moreover, heterocycles such as morpholine and thiophene were tolerated, giving rise to products **27** and **28**, respectively. The use of oxacyclic and azacyclic allenes, as well as a seven-membered carbocyclic allene, cleanly provided tricycles **29**–**32**. Furthermore, alkyl-substituted heterocyclic allenes underwent the annulation to afford products **33**–**35**. Interestingly, product **33** was obtained as a 3.8 to 1 mixture of regioisomers **33a** and **33b**, favouring formation of a fully substituted carbon (that is, **33a**), whereas products **34** and **35** were obtained as single regioisomers favouring the opposite sense of regiochemistry, an aspect of selectivity that is at present not well understood. The results shown in Fig. 2 establish the racemic methodology and demonstrate that, despite their high reactivity, strained cyclic allenes can be employed in synthetically useful transition metal-catalysed reactions, a finding that is expected to considerably expand the scope of products accessible from this class of intermediates. This transformation also provides a modular route to access phenanthridinone scaffolds, which complements existing strategies. We note that phenanthridinone frameworks are seen in biologically active compounds, such as the amaryllidaceae alkaloids, which have been explored as anti-cancer compounds[39].

Following the development of the racemic variant, we sought to identify a chiral ligand capable of rendering the transformation enantioselective. We examined the annulation of **36** with cyclic allene precursors **8** using a variety of chiral ligands and reaction conditions (see Supplementary Information, part I, section C for details), with select key results for the carbocyclic allene precursor **37** shown in Fig. 3a. The use of Quinap (**L1**), which has been used previously in a related transformation of linear allenes[40], provided poor enantioselectivity and low yield (entry 1). The DuPhos (**L2**) ligand gave the desired product (−)-**21** in 61% enantiomeric excess (e.e.), albeit in low yield (entry 2). Increased yields and enantioselectivities were observed with either Walphos ligand **L3** or BOX ligand **L4** (entries 3 and 4, respectively). The Josiphos ligand **L5** provided superior enantioselectivity, delivering (−)-**21** in 90% e.e., albeit with only 37% yield (entry 5). Further optimization revealed that reducing the ligand loading from 10 mol.% to 5 mol.% led to an increased yield of 70% (entry 6), presumably by suppressing ligand-mediated decomposition of the product, based on control experiments. To increase the conversion of silyl triflate **37**, we also examined the influence of additives. The addition of an excess of tetrabutylammonium iodide (TBAI), intended to increase the rate of allene formation by improving fluoride solubility[41], gave (−)-**21** in increased yield (entry 7) (the use of TBAF directly did not result in the desired product, see Supplementary Information part I, section C for details). Finally, by lowering the reaction temperature to 3 °C and extending the reaction time to 24 h, (−)-**21** was obtained in 85% yield and 94% e.e. (entry 8).

Having optimized the asymmetric transformation, we evaluated the scope of the methodology with respect to both the benzotriazinone and silyl triflate (Fig. 3b). Beginning with the parent substrate combination, (−)-**21** could be isolated in 85% yield and 94% e.e.. Variation of the benzotriazinone *N*-substituent was tolerated, as seen by the formation of annulation products (−)-**38**, (−)-**22**, (−)-**23**, (−)-**39**, and (−)-**24** in good yields and with high selectivities. The synthesis of (−)-**23** and (−)-**24** demonstrate the methodology's tolerance towards *N*-alkyl substituents, whereas (−)-**39** and (−)-**24** bear removable *N*-protecting groups. Heterocyclic allenes could also be employed in the asymmetric reaction. Interception of azacyclic allenes bearing either a Boc or Cbz group gave rise to enantioenriched products (−)-**31** and (−)-**30**, respectively. Similarly, the use of an oxacyclic allene delivered adduct (−)-**29** in 81% e.e.. One final example highlights the reaction between an *N*-benzyl benzotriazinone and an *N*-Boc cyclic allene to provide enantioenriched (−)-**40**, which bears differing *N*-substituents for orthogonal *N*-deprotection.

Using density functional theory, we computationally studied the mechanism of the reaction between metallacycle **41** and allenes **4** and **ent-4** catalysed by Ni/(*S*)-(*R*)-Josiphos in MeCN (Fig. 4). Density functional theory calculations have been established as a viable computational tool to assess mechanistic aspects of strained cyclic allene reactions[27] and nickel-catalysed denitrogenative processes[37]. Metallacycles analogous to **41** have previously been established as intermediates in related annulations[37]. Additionally, formation of **4** from the corresponding silyl triflate is believed to occur readily, and alternative pathways involving direct oxidative addition into the silyl triflate rather than allene formation were ruled out on the basis of calculations showing this to be kinetically implausible (see Supplementary Information part II, section C for details regarding oxidative addition into the

silyl triflate). Our first objective was to investigate the hypothesized DKR of the cyclic allene intermediate, which would require facile racemization of allene **4** and efficient discrimination of the two enantiomers by reaction with catalytically generated metallacycle **41** (Fig. 4a). Although the racemization of strained cyclic allenes can occur readily[27,33], kinetic differentiation of two strained cyclic allene enantiomers by a metal complex is unknown. Our calculations identified **TS-1** ($\Delta G^{\ddagger}$ = 7.5 kcal mol^{-1}) and **TS-1a** ($\Delta G^{\ddagger}$ = 14.9 kcal mol^{-1}) as the lowest-energy transition states for the reaction of **41** with **4** and **ent-4**, respectively, via an olefin insertion step (for details concerning reversible precomplexation of **41** and **4**/**ent-4**, see Supplementary Information part II, section A.ii.). In these competing transition states, **TS-1** is 7.4 kcal mol^{-1} lower in free energy than **TS-1a**, which is predicted to furnish intermediate metallacycle **42** in preference to stereoisomer **43**. Distortion/interaction-activation strain analysis[42] (Fig. 4b) of the two competing transition states suggests that the energy difference mainly originates from decreased distortion of the allene ($\Delta\Delta E_{\text{dist, allene}}^{\ddagger}$ = −5.3 kcal mol^{-1}) and increased interaction energy ($\Delta\Delta E_{\text{int}}^{\ddagger}$ = −4.7 kcal mol^{-1}) in **TS-1** relative to **TS-1a**. The increased allene distortion in **TS-1a** can be explained by the steric repulsion between the terminal allenic C–H bond and the cyclohexyl group on the Josiphos ligand.

Although our computational studies suggest that the enantiomers of cyclic allene **4** can be kinetically differentiated during reaction with metal complex **41**, two concerns were apparent. With the assumption that metallacycles **42** and **43** could undergo direct reductive elimination, the computationally predicted e.e. for intermediate **42** (>99% e.e. [at 3 °C], $\Delta\Delta G^{\ddagger}$ = 7.4 kcal mol^{-1}) is much higher than the experimentally observed e.e. for the final product (−)-**21** (94% e.e., $\Delta\Delta G^{\ddagger}$ = 1.9 kcal mol^{-1}). Upon validating the absolute stereochemistry of our annulation products (see Supplementary Information part I, section D for crystallographic data), we also found that direct reductive elimination from favoured intermediate **42** would provide the opposite enantiomer of the product (that is, (+)−**21**) compared to what is observed experimentally (that is, (−)-**21**). To probe this discrepancy, we calculated the kinetic barrier for direct reductive elimination of metallacycle **42** to give product (+)−**21** (Fig. 4c). Indeed, a prohibitively high barrier of 37.1 kcal mol^{-1} was found for **TS-2**, confirming that direct reductive elimination is not operative.

A plausible mechanism for the conversion of favoured metallacycle **42** to the observed annulated product (−)-**21** was subsequently investigated (Fig. 4c). More specifically, we evaluated whether the η^1-coordinated metallacycle **42** could give rise to a zwitterionic η^3-allylnickel complex **44**, which could then undergo addition at either C1 or C3 to construct the C–N bond in **21**. Metallacycle **42** can undergo facile conversion to **44**, which is a low-energy resting state. This η^1-to-η^3 isomerization ablates the stereocentre set in the olefin insertion step, leading to a prochiral π-allyl fragment. The subsequent desymmetrizing outer-sphere nucleophilic attack by the amidate anion can occur at C1 or C3, via **TS-3** (12.9 kcal mol^{-1}) or **TS-3a** (14.4 kcal mol^{-1}), leading to (−)-**21** and (+)−**21**, respectively. The calculated $\Delta\Delta G^{\ddagger}$ of 1.5 kcal mol^{-1} for these competing transition states predicts that (−)-**21** would be formed in 87% e.e. (calculated for 3 °C), which is in good agreement with the experimentally observed formation of (−)-**21** in 94% e.e. The difference in free energy between **TS-3** and **TS-3a** is hypothesized to arise from solvation differences between these

highly polar transition states (Fig. 4d). In the case of **TS-3**, the transition state is lower in energy due to a solvent-accessible cavity between the ligand's phenyl groups, which allows solute-solvent interactions that stabilize the amidate anion. In **TS-3a**, the bulky cyclohexyl (Cy) groups on the Josiphos ligand sterically shield the amidate from the solvent, causing **TS-3a** to be comparatively less stable and therefore higher in energy. This hypothesis is further supported by calculations showing that changing the cyclohexyl substituent to less sterically demanding groups lowers the $\Delta\Delta G^{\ddagger}$ value, as well as gas-phase calculations demonstrating that **TS-3** is less favourable than **TS-3a** in the absence of solvent effects (see Supplementary Information part II, section B for additional computational details on solvent effects).

Overall, the computational results indicate a mechanism (summarized in Extended Data Fig. 1) involving: (1) kinetic differentiation of the cyclic allene enantiomers **4** through stereoselective olefin insertion with **41**, (2) subsequent loss of stereochemical information by formation of η^3-allylnickel complex **44**, and (3) stereoselective outer-sphere attack at C1 to give (−)-**21**. Thus, in future reaction design, one may consider either kinetic differentiation of cyclic allene enantiomers or the intentional formation of η^3-allylmetal intermediates as viable means of introducing absolute stereochemistry in reactions of strained cyclic allenes.

Extended Data

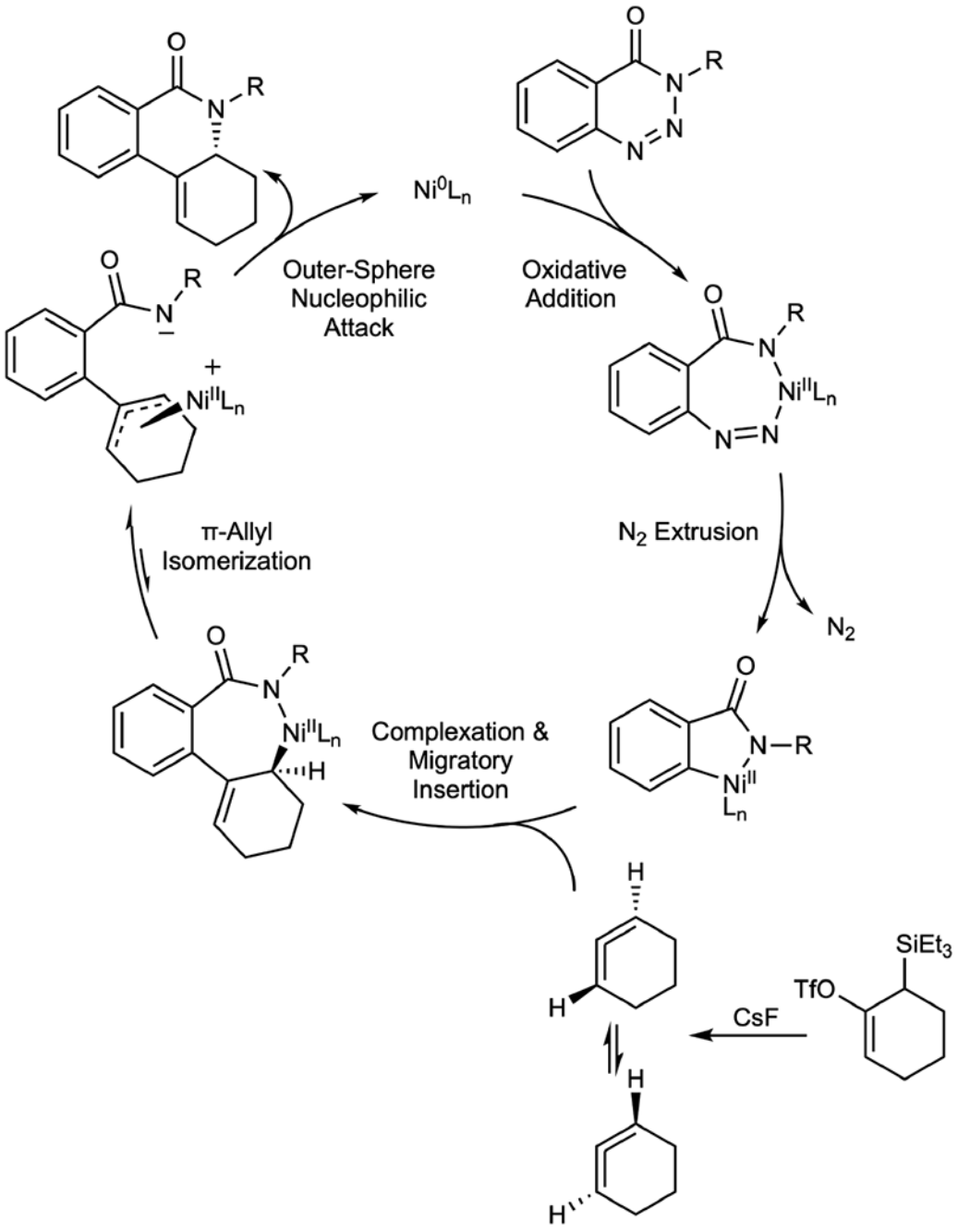

Extended Data Fig. 1|. Proposed catalytic cycle.

Computational studies support a mechanism involving activation of the benzotriazinone by the Ni catalyst, migratory insertion across one olefin of the cyclic allene, isomerization to a Ni π-allyl complex, and enantioselective outer-sphere attack to provide the observed phenanthridinone.

Supplementary Material

Refer to Web version on PubMed Central for supplementary material.

Acknowledgements

We are grateful to the NIH-NIGMS (R01 GM123299 and R01 GM132432 for N.K.G., and T32 GM067555 for A.V.K.), the NSF (CHE-1764328 for K.N.H., DGE-1144087 for M.M.Y. and B.J.S., and DGE-1650604 for A.V.K.), the Trueblood family (for N.K.G.), and the Swiss National Science Foundation for an Early Mobility Postdoctoral Fellowship (M.G.). These studies were supported by shared instrumentation grants from the NSF (CHE-1048804) and the NIH NCRR (S10RR025631). Calculations were performed on the Hoffman2 cluster and the UCLA Institute of Digital Research and Education (IDRE) at UCLA and the Extreme Science and Engineering Discovery Environment (XSEDE), which is supported by the National Science Foundation (OCI-1053575).

Data availability

Crystallographic data are available free of charge from the Cambridge Crystallographic Data Centre under CCDC 1987661. The authors declare that all other data supporting the findings of this study are available within the paper and its Supplementary Information files.

References

1. Wenk HH, Winkler M & Sander W One century of aryne chemistry. Angew. Chem. Int. Ed 42, 502–528 (2003).
2. Liebman JF & Greenberg A A survey of strained organic molecules. Chem. Rev 76, 311–365 (1976).
3. Angus RO Jr, Schmidt MW & Johnson RP Small-ring cyclic cumulenes: theoretical studies of the structure and barrier to inversion of cyclic allenes. J. Am. Chem. Soc 107, 532–537 (1985).
4. Pellissier H & Santelli M The use of arynes in organic synthesis. Tetrahedron 59, 701–730 (2003).
5. Dockendorff C, Sahli S, Olsen M, Milhau L & Lautens M Synthesis of dihydronaphthalenes via aryne-Diels–Alder reactions: scope and diastereoselectivity. J. Am. Chem. Soc 127, 15028–15029 (2005). [PubMed: 16248633]
6. Picazo E et al. Arynes and cyclic alkynes as synthetic building blocks for stereodefined quaternary centers. J. Am. Chem. Soc 140, 7605–7610 (2018). [PubMed: 29716194]
7. Stoermer R & Kahlert B Ueber das 1-Brom-cumaron. Ber. Dtsch. Chem. Ges 35, 1633–1640 (1902).
8. Roberts JD, Simmons HE, Carlsmith LA & Vaughan CW Rearrangement in the reaction of chlorobenzene-1-C^{14} with potassium amide. J. Am. Chem. Soc 75, 3290–3291 (1953).
9. Wittig G Phenyl-lithium, der Schlüssel zu einer neuen Chemie metallorganischer Verbindungen. Naturwissenschaften 30, 696–703 (1942).
10. Wittig G & Pohmer L Intermediäre Bildung von Dehydrobenzol (Cyclohexa-dienin). Angew. Chem 67, 348 (1955).
11. Scardiglia F & Roberts JD Evidence for cyclohexyne as an intermediate in the coupling of phenyllithium with 1-chlorocyclohexene. Tetrahedron 1, 343–344 (1957).
12. Wittig G & Fritze P On the intermediate occurrence of 1,2-cyclohexadiene. Angew. Chem. Int. Edn Engl 5, 846 (1966).
13. Berry RS, Clardy J & Schafer ME Benzyne. J. Am. Chem. Soc 86, 2738–2739 (1964).
14. Diau EW-G, Casanova J, Roberts JD & Zewail AH Femtosecond observation of benzyne intermediates in a molecular beam: Bergman rearrangement in the isolated molecule. Proc. Nat. Acad. Sci. 97, 1376–1379 (2000). [PubMed: 10660684]
15. Dubrovskiy AV, Markina NA & Larock RC Use of benzynes for the synthesis of heterocycles. Org. Biomol. Chem 11, 191–218 (2013). [PubMed: 23132413]
16. Chen S et al. Preparation of substituted 2,2-bipyrimidinyl compounds and analogs thereof, and methods using the same. International patent W02019222238 A2 (2019).

17. Mauger CC & Mignani GA An efficient and safe procedure for the Large-scale Pd-catalyzed hydrazonation of aromatic chlorides using Buchwald technology. Org. Process Res. Dev 8, 1065–1071 (2004).
18. Takikawa H, Nishii A, Sakai T & Suzuki K Aryne-based strategy in the total synthesis of naturally occurring polycyclic compounds. Chem. Soc. Rev 47, 8030–8056 (2018). [PubMed: 30357181]
19. Tadross PM & Stoltz BM A comprehensive history of arynes in natural product total synthesis. Chem. Rev 112, 3550–3577 (2012). [PubMed: 22443517]
20. Gampe CM & Carreira EM Arynes and cyclohexyne in natural product synthesis. Angew. Chem. Int. Ed 51, 3766–3778 (2012).
21. Schleth F, Vettiger T, Rommel M & Tobler H Process for the preparation of pyrazole carboxylic acid amides. International patent WO2011131544 A1 (2011).
22. Lin JB, Shah TJ, Goetz AE, Garg NK & Houk KN Conjugated trimeric scaffolds accessible from indolyne cyclotrimerizations: synthesis, structures, and electronic properties. J. Am. Chem. Soc 139, 10447–10455 (2017). [PubMed: 28675700]
23. Caeiro J, Peña D, Cobas A, Pérez D & Guitián E Asymmetric catalysis in the [2+2+2] cycloaddition of arynes and alkynes: enantioselective synthesis of a pentahelicene. Adv. Synth. Catal 348, 2466–2474 (2006).
24. Yubuta A et al. Enantioselective synthesis of triple helicenes by cross-cyclotrimerization of a helicenyl aryne and alkynes via dynamic kinetic resolution. J. Am. Chem. Soc 142, 10025–10033 (2020). [PubMed: 32390427]
25. Li L, Li Y, Fu N, Zhang L & Luo S Catalytic asymmetric electrochemical α-arylation of cyclic (β-ketocarbonyls with anodic benzyne intermediates. Angew. Chem. Int. Ed 59, 14347–14351 (2020).
26. Quintana I, Peña D, Pérez D & Guitián E Generation and reactivity of 1,2-cyclohexadiene under mild reaction conditions. Eur. J. Org. Chem 2009, 5519–5524 (2009).
27. Barber JS et al. Diels–Alder cycloadditions of strained azacyclic allenes. Nat. Chem 10, 953–960 (2018). [PubMed: 30061614]
28. Lofstrand VA & West FG Efficient trapping of 1,2-cyclohexadienes with 1,3-dipoles. Chemistry 22, 10763–10767 (2016). [PubMed: 27219685]
29. Barber JS et al. Nitrone cycloadditions of 1,2-cyclohexadiene. J. Am. Chem. Soc. 138, 2512–2515 (2016). [PubMed: 26854652]
30. Yamano MM et al. Cycloadditions of oxacyclic allenes and a catalytic asymmetric entryway to enantioenriched cyclic allenes. Angew. Chem. Int. Ed 58, 5653–5657 (2019).
31. Lofstrand VA, McIntosh KC, Almehmadi YA & West FG Strain-activated Diels–Alder trapping of 1,2-cyclohexadienes: intramolecular capture by pendent furans. Org. Lett 21, 6231–6234 (2019). [PubMed: 31343882]
32. Pellissier H Dynamic kinetic resolution. Tetrahedron 59, 8291–8327 (2003).
33. Balci M & Jones WM Chirality as a probe for the structure of 1,2-cycloheptadiene and 1,2-cyclohexadiene. J. Am. Chem. Soc 102, 7607–7608 (1980).
34. Dhokale RA & Mhaske SB Transition-metal-catalyzed reactions involving arynes. Synthesis 50, 1–16 (2018).
35. Chattopadhyay B & Gevorgyan V Transition-metal-catalyzed denitrogenative transannulation: converting triazoles into other heterocyclic systems. Angew. Chem. Int. Ed 51, 862–872 (2012).
36. Thorat VH, Upadhyay NS, Murakami M & Cheng C-H Nickel-catalyzed denitrogenative annulation of 1,2,3-benzotriazin-4-(3*H*)-ones with benzynes for construction of phenanthridinone scaffolds. Adv. Synth. Catal 360, 284–289 (2018).
37. Wang N, Zheng S-C, Zhang L-L, Guo Z & Liu X-Y Nickel(0)-catalyzed denitrogenative transannulation of benzotriazinones with alkynes: mechanistic insights of chemical reactivity and regio- and enantioselectivity from density functional theory and experiment. ACS Catal. 6, 3496–3505 (2016).
38. Yamauchi M, Morimoto M, Miura T & Murakami M Enantioselective synthesis of 3,4-dihydroisoquinolin-1(2*H*)-ones by nickel-catalyzed denitrogenative annulation of 1,2,3-benzotriazin-4(3*H*)-ones with allenes. J. Am. Chem. Soc 132, 54–55 (2010). [PubMed: 20000760]

39. Jin Z & Yao G Amaryllidaceae and sceletium alkaloids. Nat. Prod. Rep 36, 1462–1488 (2019). [PubMed: 30707215]

40. Miura T, Yamauchi M, Kosaka A & Murakami M Nickel-catalyzed regio- and enantioselective annulation reactions of 1,2,3,4-benzothiatriazine-1,1(2*H*)-dioxides with allenes. Angew. Chem. Int. Ed 49, 4955–4957 (2010).

41. Feng M, Tang B, Wang N, Xiu H-X & Jiang X Ligand controlled regiodivergent C1 insertion on arynes for construction of phenanthridinone and acridone alkaloids. Angew. Chem. Int. Ed 54, 14960–14964 (2015).

42. Bickelhaupt FM & Houk KN Analyzing reaction rates with the distortion/interaction activation strain model. Angew. Chem. Int. Ed 56, 10070–10086 (2017).

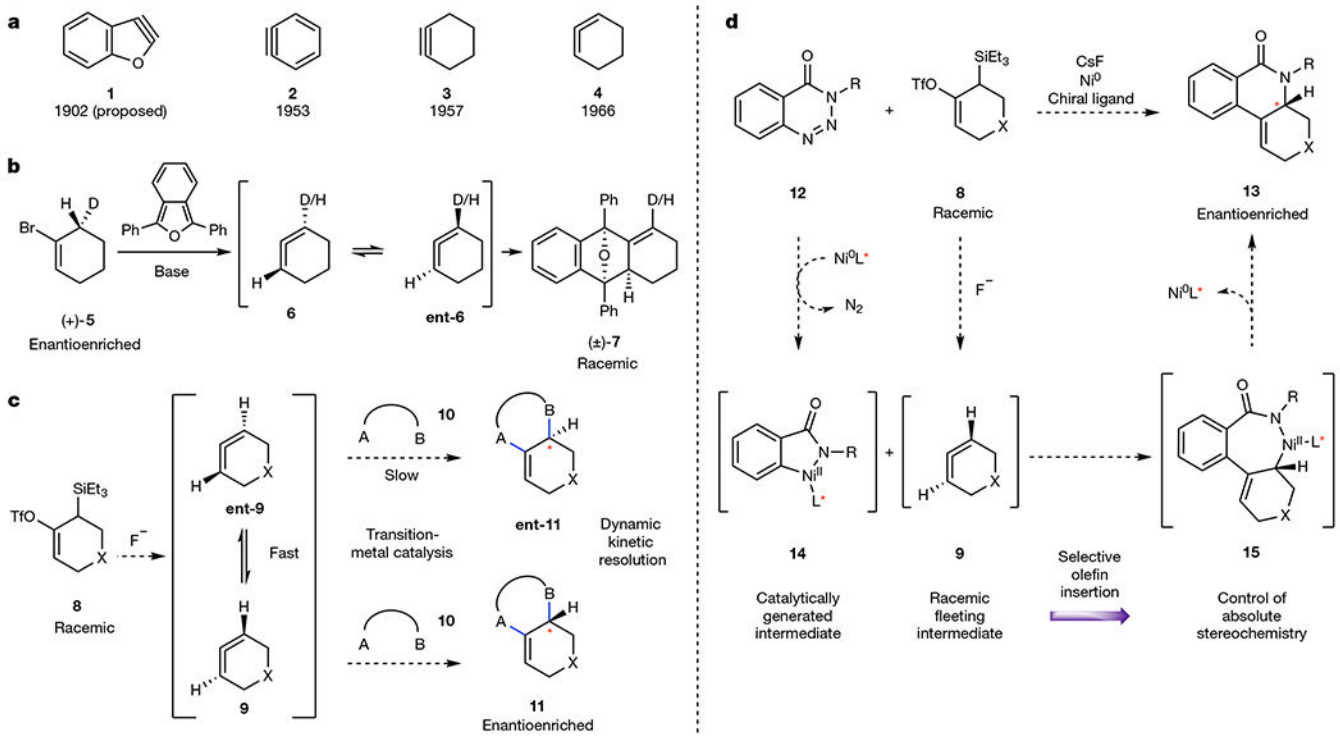

Fig. 1|. Historical context of strained cyclic intermediates and current reaction design.

a, Milestones in strained cyclic intermediate chemistry. **b**, Seminal report of strained cyclic allene racemization, wherein an enantioenriched cyclic allene precursor is converted to a racemic cycloadduct. **c**, Our reaction design wherein a racemic cyclic allene precursor would be converted to an enantioeriched annulated product via the dynamic kinetic resolution of strained cyclic allene intermediates. **d**, Envisioned reaction pathway delivering enantioenriched products through a stereoselective olefin insertion reaction. Ph, phenyl; OTf, trifluoromethanesulfonate; Et, ethyl; X, CH_2, $(CH_2)_2$, *N*-Boc, *N*-Cbz, or O; A, carbon substituent; B, nitrogen substituent; R, aryl or alkyl group; L*, chiral ligand.

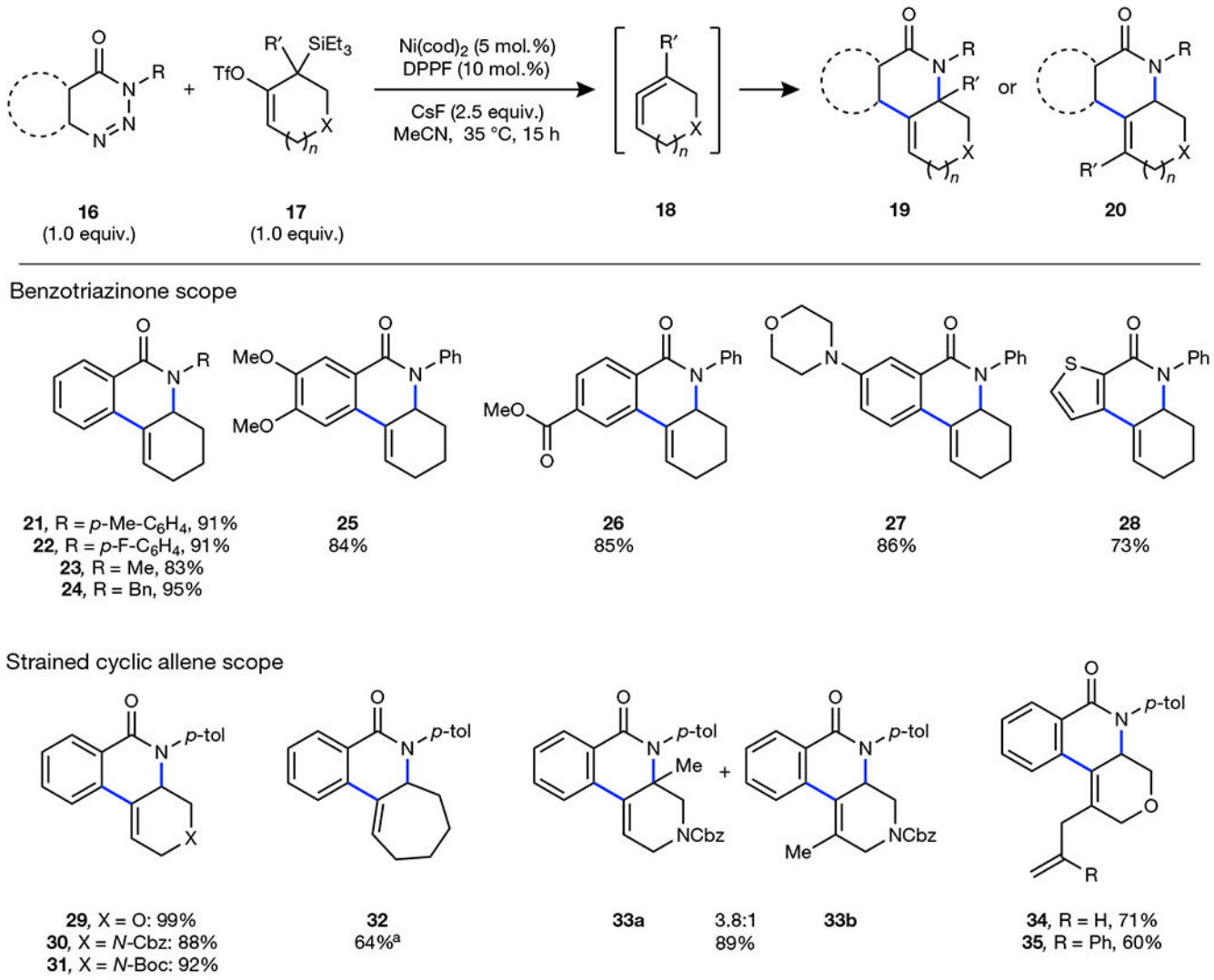

Fig. 2|. Scope of benzotriazinones and cyclic allenes in the racemic annulation reaction.

Yields shown reflect an average of two isolation experiments. [a]Reaction was run for 40 h using a silyl tosylate as a cyclic allene precursor. R, aryl or alkyl; R′, H or alkyl; OTf, trifluoromethanesulfonate; X, CH_2, $(CH_2)_2$, *N*-Boc, *N*-Cbz, O; Et, ethyl; cod, 1,5-cyclooctadiene; DPPF, 1,1′-bis(diphenylphosphino)ferrocene; Me, methyl; Bn, benzyl; Ph, phenyl; *p*-tol, *p*-Me-C_6H_4; Cbz, carboxybenzyl; Boc, *tert*-butyloxycarbonyl.

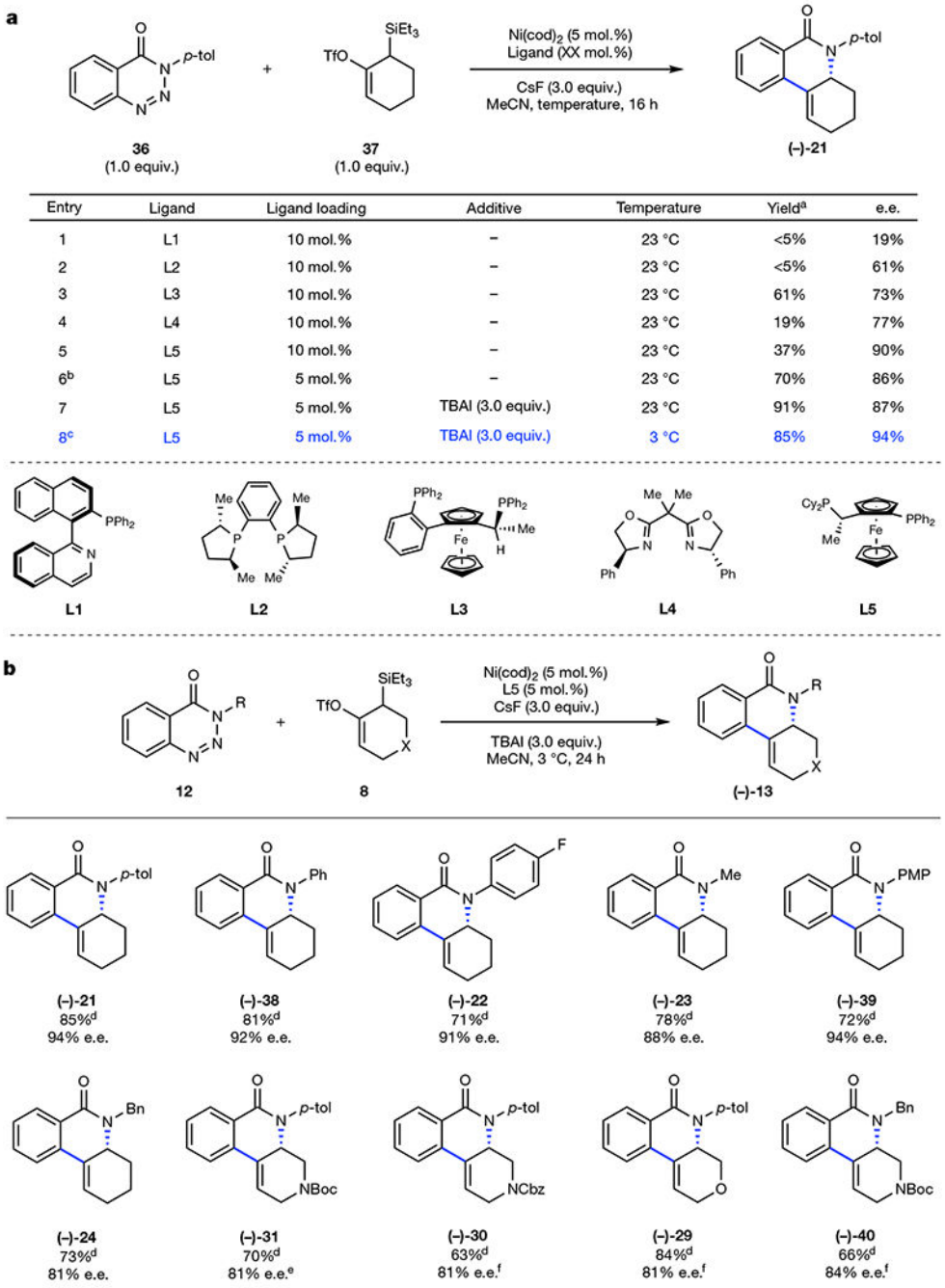

Entry	Ligand	Ligand loading	Additive	Temperature	Yield[a]	e.e.
1	L1	10 mol.%	–	23 °C	<5%	19%
2	L2	10 mol.%	–	23 °C	<5%	61%
3	L3	10 mol.%	–	23 °C	61%	73%
4	L4	10 mol.%	–	23 °C	19%	77%
5	L5	10 mol.%	–	23 °C	37%	90%
6[b]	L5	5 mol.%	–	23 °C	70%	86%
7	L5	5 mol.%	TBAI (3.0 equiv.)	23 °C	91%	87%
8[c]	L5	5 mol.%	TBAI (3.0 equiv.)	3 °C	85%	94%

(–)-21 85%[d] 94% e.e. | (–)-38 81%[d] 92% e.e. | (–)-22 71%[d] 91% e.e. | (–)-23 78%[d] 88% e.e. | (–)-39 72%[d] 94% e.e.

(–)-24 73%[d] 81% e.e. | (–)-31 70%[d] 81% e.e.[e] | (–)-30 63%[d] 81% e.e.[f] | (–)-29 84%[d] 81% e.e.[f] | (–)-40 66%[d] 84% e.e.[f]

Fig. 3|. Optimization and scope of the asymmetric annulation.

a, Optimization of the asymmetric annulation. **b**, Scope of the asymmetric annulation reaction. [a]Yields were determined by ^{1}H NMR analysis of the crude reaction mixture using 1,3,5-trimethoxybenzene as an external standard. [b]Empirically, it was found that a 1:1 ratio of nickel to Josiphos ligand gave higher yields of product. Control experiments showed that product **21** undergoes non-specific decomposition in the presence of unligated Josiphos. However, we cannot discount the possibility that with a 1:2 ratio of Ni:Josiphos ligand, a less reactive, saturated Ni(Josiphos)$_2$ complex could also form, potentially further

decreasing reaction efficiency. [c]Reaction was performed for 24 h. [d]Yield was determined by an isolation experiment. [e]Reaction was performed with 10 mol.% $Ni(cod)_2$ and 10 mol.% of L5 in the absence of TBAI. [f]Reaction was performed with 10 mol.% $Ni(cod)_2$ and 10 mol.% of L5 in the absence of TBAI at 23 °C. TBAI, tetrabutylammonium iodide; X, *N*-Boc, *N*-Cbz, or CH_2; PMP, *p*-methoxyphenyl.

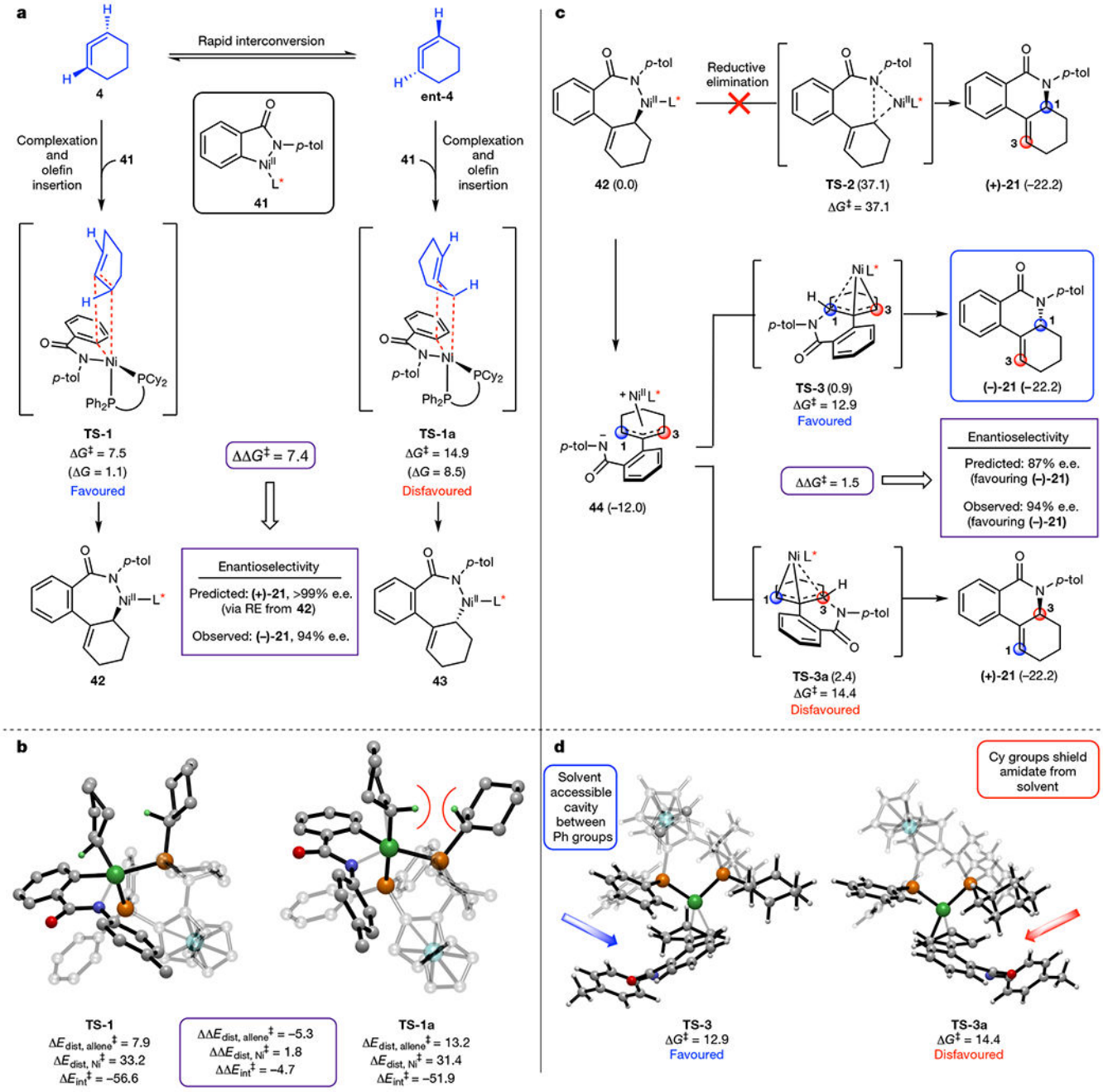

Fig. 4|. Computational study of the asymmetric annulation reaction mechanism.

a, Reaction pathway and calculated transition state barriers for the olefin insertion step. A precomplex is formed reversibly by the allene and Ni before the insertion, and the reported $\Delta G^{\ddagger}$ values are relative to the lowest energy allene-Ni complex (see Supplementary Information part II and Supplementary Fig. 5). Free energies relative to uncomplexed **41** and **4** (ΔG) are noted in parentheses. **b**, Optimized transition state structures **TS-1** and **TS-1a** and distortion interaction analysis for the olefin insertion. **c**, Possible pathways from **42** to (−)-**21**/(+)−**21**. Calculated free energies relative to **42** are indicated in parentheses. **d**, Optimized transition state structures **TS-3** and **TS-3a** for the outer-sphere nucleophilic

attack. Calculations were performed at the M06L/6-311++G(d,p), SDD(Ni, Fe)/SMD(MeCN)//B3LYP-D3(BJ)/6-31G(d), LANL2DZ(Ni, Fe)/SMD(MeCN) level. All energies are reported in kilocalories per mole. L*, (*S*)-(*R*)-Josiphos; RE, reductive elimination.